Korean J. Chem. Eng., 38(8), 1578-1591 (2021)
DOI: 10.1007/s11814-021-0818-0

pISSN: 0256-1115
eISSN: 1975-7220

Pressure drop axial distribution uniformity of the particle bed in the radial bed

Tianhang Wu*, Dewu Wang*,, Ruojin Wang*,†, Bin Zhao*,†, Meng Tang***, Shaofeng Zhang*,**, and Lu Nie***

*School of Chemical Engineering and Technology, Hebei University of Technology, Tianjin 300130, China
**National and Local Joint Laboratory for Chemical Energy Conservation Process Integration and Resource Utilization, Tianjin 300130, China
***School of Mechanical Engineering, Hebei University of Technology, Tianjin 300130, China
(*Received 19 January 2021 • Revised 3 April 2021 • Accepted 23 April 2021*)

Abstract−In a radial bed, the uniformity of the pressure drop distribution is investigated by Euler single-phase flow and porous media models under different operating mode (CF-U/Z, CP-U/Z), gas flow rate (120-240 m^3/h), particle diameter ((0.5-3)exp-3 m) and bed voidage (0.3-0.6). According to the nonuniform index η, the uniformity relates to these parameters and improves with increasing total pressure drop of particle bed Δp_s (sum of the pressure drops of particle bed and gas perforation) or decreasing main channel pressure drop Δp_g. Comparing the flow fields with/without particles, Δp_s is approximately equal to the pressure drop of the particle bed with high-porosity Johnson net, which is well calculated by the Ergun equation. Δp_g can be calculated by the modified momentum equation containing k. After changing the wall shear stress and gas-solid axial resistance, it is found that the internal generation factors for k include the influence of gas perforation on boundary layer and the existence of gas axial velocity after perforation. Besides, the global/local k hardly changes with the investigated parameters. The local k is a function of axial position or velocity ratio, which changes obviously at the end of the main channel for the existence of a gas stagnation zone.

Keywords: Radial Bed, Pressure Drop Distribution, Particle Bed, Main Channel, Momentum Exchange Coefficient

INTRODUCTION

In a radial bed, the fluid is fed to the discharge channel, which flows along the axial direction, simultaneously enters the particle bed through the holes in the pipe wall, collects in the collection channel and subsequently exits from the bed. In a particle bed, the fluid flow cross-section is a cylinder with a large area, which gives the fluid flow cross-section the advantages of a low pressure drop, a large gas handling capacity and the ease of up scaling [1-3]. A radial bed has been widely used in many industrial processes, e.g., the synthesis of ammonia [4], catalytic reforming [5], rapid gas-solid catalysis [6], and propane dehydrogenation [7].

In the discharge/collection channels, when the fluid is moving along the axial direction, its flow rate continuously changes as the fluid flows into/out of the channel through the wall holes. That process is called variable mass flow. For the normal-/low-pressure radial flow reactors, the dynamic pressure at the end of the radial bed should be less than 20-50 kg/m^2 (17.89-28.28 m/s) [8]. The gas velocity is so high that the pressure changes caused by the variable mass flow result in a difference in pressure between two channels. Similar to the gas distributor [9] and manifold system [10,11], the axial change of pressure in the main channels usually causes the nonuniform distribution of the pressure drop in the particle bed, which can seriously affect the bed performance [12-14]. The bed performance is usually represented by the pressure and velocity distribution in the radial bed. Due to the small gas velocity in the particle bed and large variation in gas velocity in the channels, it is difficult to obtain the exact gas velocity value in the radial bed, which makes the investigation of the pressure distribution a good choice. Since the pressure drop in the particle bed is commonly represented by the pressure difference between two channels, compared to the gas velocity the pressure variation in the channels is studied by many researchers.

Many equations have been established to calculate the pressure change in the main channels, e.g., Bernoulli, modified momentum and total energy equations. The modified momentum equation with momentum exchange coefficient k [15-17] has been widely used. The parameters in Eq. (1) are the pressure change, gravity, momentum exchange and frictional resistance. When the fluid flow direction is identical to or different from the gravity direction, the gravity term is taken as "−" or "+". For the discharge/collection channel, the friction resistance term is taken as "+" or "−" [18]. The friction resistance coefficient is calculated by Eq. (2). k reflects the effect of the gas flow through the holes on the boundary layer. Currently, k is usually obtained by the reverse derivation of the pressure and velocity. Early scholars gave the k calculation formula based on the gas velocity ratio of the main channel before/after the holes in porous tubes [8,15,19]. Similarly, later scholars provided the calculation formula based on the gas velocity ratio before/after the holes [12] u′/u″ or the relative change rate of kinetic energy in the radial bed (du/dz)/u [16]. k is only a function of the gas velocity ratio and independence of the gas velocity, the operating mode and the structural dimension. In addition to calculating the pressure change in the main channel, k can be used in the optimal design of the radial bed [20,21]. For example, in the design of variable-cross-section flow channel structures such as conical and

†To whom correspondence should be addressed.
E-mail: wangrj@hebut.edu.cn, hgdzhaobin@163.com

choke devices, the pressure change term in formula (1) can be assumed to be zero. Using k, the local gas velocity at different axial heights can be obtained to determine the axial position of the flow cross-sectional area and size. Recently, k was found to relate to the axial position [17]. Detailed information remains to be explored, e.g., its internal causes and the effects of different operating/gas-solid parameters.

$$\frac{dp}{dz} \pm \rho g\left(1-\frac{du}{2u}\right)dz + 2k\rho u\frac{du}{dz} \mp \frac{\lambda(1-\phi)}{2D_e}\rho u^2 = 0 \quad (1)$$

$$\begin{cases} \lambda = \dfrac{u\rho D_e}{\mu} & Re \le 4{,}000 \\ \dfrac{1}{\sqrt{\lambda}} = -2\lg\left(\dfrac{2.51}{Re\sqrt{\lambda}} + \dfrac{d'}{3.7D_e}\right) & Re > 4{,}000 \end{cases} \quad (2)$$

The uniformity of the particle bed pressure drop distribution is affected by the pressure change in the main channel and total pressure drop of the particle bed (sum of the gas perforation and particle bed pressure drop). This effect is easily ignored by some researchers, whose goal is only to reduce the pressure variation in the channels. The pressure change in the main channel can be ignored under small gas perforation or large particle bed pressure drop. The variable porosity (including unilateral/bilateral variable porosity regulation) optimization method [17,22-24] improves the total pressure drop mainly by increasing the gas perforation pressure drop but increases the energy resources. Thus, a Johnson net with high porosity is used to reduce the pressure drop here, and the value can be determined in the empty radial bed. The pressure drop of a particle bed comes from the gas-solid collision and friction, which relates to the gas velocity, particle diameter, bed voidage and other parameters [25-29], considering that the local gas velocity in the particle bed is much lower than the local gas velocity in the main channel. Although many particles accumulate in the particle bed, its pressure drop is hardly much larger than the pressure drop of the main channel. To better explain the relationship of the pressure distribution uniformity to the pressure change in the main channel and total pressure drop of the particle bed, the flow field must be studied under different operating/gas-solid parameters in the radial bed.

In conclusion, the distribution uniformity of the pressure drop in the particle bed is affected by the total pressure drop of the bed and pressure change in the main channels. In this paper, the gas flow field was investigated under different operating mode, gas flow rate, particle diameter and bed voidage. After comparing the flow fields in the bed with/without particles under different conditions, the pressure drop of gas perforation, particle bed and entire bed was analyzed. The pressure drop distribution is discussed for its average value and uniformity. To analyze the pressure change in the channels, the relationship and difference of the flow field were analyzed in depth in the upper, middle and lower parts of the main channel. The internal factors of the momentum exchange coefficient k were analyzed by changing the wall shear stress and gas-solid axial resistance. The change rules of global and local k were also studied.

NUMERICAL SIMULATION

The radial bed in the literature [17] was selected as the simulation object. After performing grid independence, turbulence model selection and model verification, the pressure drop distribution uniformity was qualitatively and quantitatively analyzed under different conditions in the particle bed.

1. Modeling and Meshing

A radial bed consists of discharge/collection channels and a particle bed, which are separated by a Johnson net, as shown in Fig. 1.

A radial bed contains gas and solid phases. The gas is air at nor-

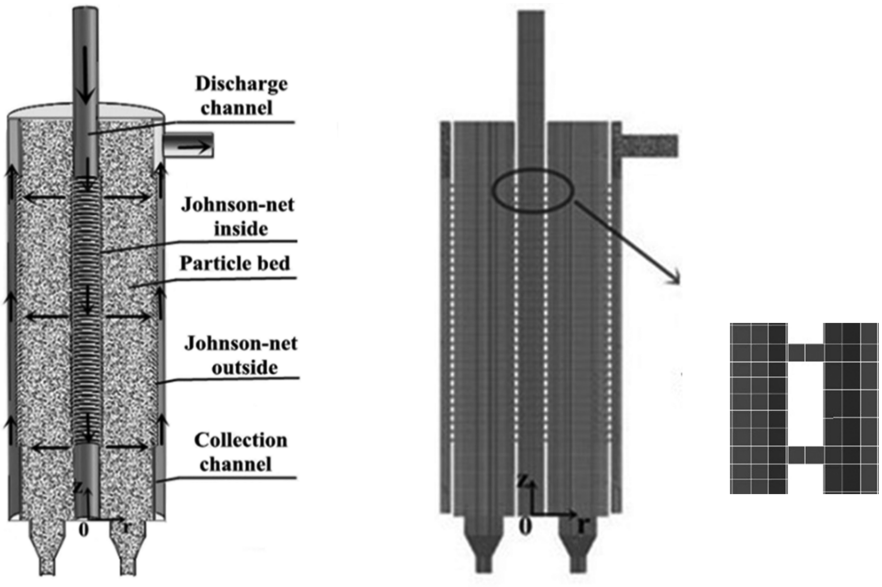

(a) Device (b) Grid

Fig. 1. Schematic diagram of device and grid in the CF-U radial bed.

Table 1. Model and simulation parameter settings

Types	Experimental parameters		value	Simulation parameters		value
Fixed parameters	Particle bed	Upper height	0.53 m	Simulation method		Euler single phase flow model
		Middle height	0.85 m			Porous media model
		Lower height	0.225 m	Turbulence model		k-ε RNG
		Inner diameter	0.07 m	Boundary conditions	Entrance	Velocity inlet
		Outer diameter	0.43 m		Export	Pressure outlet
	Annular pipe outer diameter	0.48 m			Wall surface	Non-slip boundary condition
	Johnson net porosity	16.7%		Simulation type		Pressure-based transient
	Gas	Normal temperature and pressure air				
	Gas density	1.225 kg/m^3		Algorithm		SIMPLE
	Gas viscosity	1.79exp-5 kg/(m·s)		Max iteration		40
	Particles	Quartz sand particles		Time Step		0.0001 s
	Particle packing density	1,500 kg/m^3		Calculate the total time		1-2 s
Variable parameters	Operation mode	CF-U, CF-Z types		Operation mode		CF-U/Z types; CP-U/Z types
	Gas flow rate	120-240 m^3/h		Gas flow rate		120-240 m^3/h
	Average particle diameter	0.77exp-3 m		Average particle diameter		(0.5-3) exp-3 m
	Bed voidage	0.345		Bed voidage		0.3~0.6
	Particle accumulation	After accumulation		Particle accumulation		Before and after accumulation
	Wall boundary conditions	Experimental conditions		Wall boundary conditions		Shear conditions
	Particle bed resistance	Homogeneity		Particle bed resistance		Inertial/Viscous resistance coefficient

mal temperature and pressure, which flows through the discharge channel, particle bed and collection channel. The solids are quartz sand particles that accumulate only in the particle bed, entering into the feed port and discharging from the discharge ports. The relevant parameters are shown in Table 1.

Gambit 2.4.6 was used to perform the full-scale 3D modeling and meshing of the bed. Different meshing strategies were adopted for each part of the radial bed: tetrahedral nonstructural grids for the inlet/outlet of the annular pipe and solid discharge port and hexahedral grids for the remainder. In addition, 30 circular hole channels were used instead of the Johnson net. The same porosity is guaranteed to ensure the calculation accuracy at low computational cost.

2. Mathematical Model and Simulation Settings

In Fluent 6.3.24, Euler single-phase flow and porous media models were used. The gas mass and momentum equations are shown in Eq. (3) and Eq. (4). In Eq. (4), the stress tensor is calculated by Eq. (5). The Reynolds stress is calculated by Boussinesq assumption Eq. (6); the k-ε RNG turbulence model is adopted by Eq. (7) and Eq. (8). The source term employs the porous media model to calculate the gas-solid resistance. The inertial and viscous resistance coefficients (10) and (11) are given. The other important information is listed in Table 1.

$$\frac{\partial \gamma\rho_g}{\partial t}+\nabla\cdot(\gamma\rho_g\mathbf{u})=0 \tag{3}$$

$$\frac{\partial(\gamma\rho_g\mathbf{u})}{\partial t}+\nabla\cdot(\gamma\rho_g\mathbf{uu})=-\gamma\nabla p+\gamma\rho_g g+\gamma\nabla\cdot\bar{\bar{\tau}}+\gamma\nabla\cdot(-\rho_g\overline{\mathbf{u'u'}})+\gamma\mathbf{S}_i \tag{4}$$

$$\bar{\bar{\tau}}=\mu\left[(\nabla\mathbf{u}+\nabla\mathbf{u}^T)-\frac{2}{3}\nabla\cdot\mathbf{u}\bar{\bar{I}}\right] \tag{5}$$

$$-\rho_g\overline{u_i'u_j'}=\mu_t\left(\frac{\partial u_i}{\partial x_j}+\frac{\partial u_j}{\partial x_i}\right)-\frac{2}{3}\left(\rho\kappa+\mu_t\frac{\partial v_k}{\partial x_k}\right)\delta_{ij} \tag{6}$$

$$\frac{\partial(\rho\kappa)}{\partial t}+\frac{\partial(\rho\kappa\mathbf{u})}{\partial x}=\frac{\partial}{\partial x_j}\left[\alpha_k\mu_{eff}\frac{\partial\kappa}{\partial x_j}\right]+G_\kappa+G_b-\rho\varepsilon-Y_M \tag{7}$$

$$\frac{\partial(\rho\varepsilon)}{\partial t}+\frac{\partial(\rho\varepsilon\mathbf{u})}{\partial x}=\frac{\partial}{\partial x_j}\left[\alpha_\varepsilon\mu_{eff}\frac{\partial\varepsilon}{\partial x_j}\right]+C_{1\varepsilon}\frac{\varepsilon}{\kappa}(G_\kappa+C_{3\varepsilon}G_b)-C_{2\varepsilon}\rho\frac{\varepsilon^2}{\kappa}-R_\varepsilon \tag{8}$$

$$S_i=-\left(\frac{\mu}{\alpha}u_i+\frac{C_2}{2}\rho_g|u_i|u_i\right) \tag{9}$$

$$\frac{1}{\alpha}=\frac{150}{d_p^2}\cdot\frac{(1-\gamma)^2}{\gamma^3} \tag{10}$$

$$C_2 = \frac{3.5}{d_p} \cdot \frac{(1-\gamma)}{\gamma^3} \quad (11)$$

3. Model Validation

3-1. Grid Independence Verification

Referring to relevant studies [30-33], the mesh size was selected as 0.005, 0.01 and 0.015 m in this paper with the corresponding grid numbers of 1,715,597, 852,807 and 363,110, respectively.

As shown in Fig. 2(a), when the grid size is 0.005 and 0.01 m, both pressure drop axial distribution and gas velocity/pressure radial distribution at the axial height center z/H=0.5 are basically identical. However, there is a difference when the grid size is 0.015 m, as shown in area A in Fig. 2 because the grid size is larger than the porosity height of the Johnson net, and the flow field nearby cannot be well estimated. A grid size of 0.01 m was used here.

3-2. Turbulence Model

The local gas velocity is relatively high in the main channel with turbulent flow, while the local gas velocity is low in the particle bed with laminar flow. Then, different turbulence models are used to examine their effects.

As shown in Fig. 2(b), under four calculation models of the k-ε standard, RNG, Realizable, and RSM, both the pressure drop axial distribution and gas velocity/pressure radial distribution at z/H=0.5 are basically identical. However, the gas velocity radial distribution at z/H=0.5 in the laminar flow model is significantly different from the gas velocity radial distribution at z/H=0.5 in the other models, as shown in area B in Fig. 2(b). Because the gas remains turbulent in the main channel with a high Reynolds number, while the laminar model ignores the turbulent effect. The k-ε RNG model, which better simulates the bending flow, was used for the follow-up study.

3-3. Model Verification

The focus in this paper is the uniformity of the pressure drop/gas velocity axial distribution in the particle bed. In experiments,

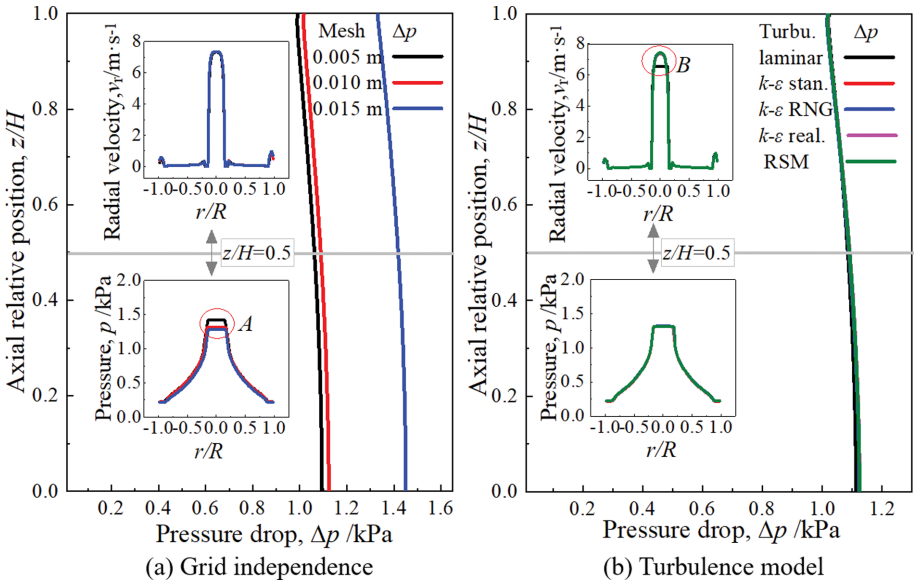

Fig. 2. Grid independence and turbulence model verification (CF-U, Q=180 m^3/h, d_p=0.77exp-3 m, γ=0.345).

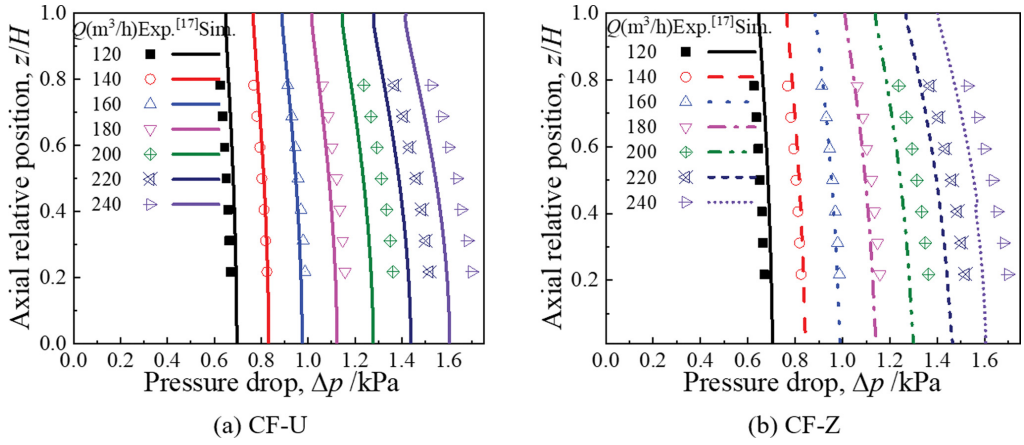

Fig. 3. Comparison of experimental and simulated results of the total pressure drop of particle bed in the CF-type radial bed (d_p=0.77exp-3 m, γ=0.345).

the gas velocity is difficult to accurately measure because it greatly changes with the radial position in the particle bed, so the pressure is often measured. The pressure drop of the bed is the difference in pressure between discharge/collection channels, which hardly changes with the radial position (section 3.1.1).

The experimental and simulation results of the pressure drop distribution in the particle bed are almost identical and the relative error is less than 10%, as shown in Fig. 3. The pressure drop distribution can be accurately obtained by simulation. The gas velocity distribution in the particle bed is obtained by simulation, which is difficult to obtain by experiments, but it is also considered to be accurate because it closely relates to the pressure drop distribution according to the Ergun equation (section 3.2.1). Thus, the gas velocity and pressure distribution in the main channels are considered to be corrected.

RESULTS AND DISCUSSION

To satisfy the technological requirements of different processes, different operations and gas/solid parameters are required. To better reveal the flow characteristics, these conditions are analyzed by the single-factor variable method.

First, the gas flow field is investigated under different conditions in both the main channels and particle bed. The main channels can be divided into discharge and collection channels according to their functions or center and annular pipes according to their positions. Second, the pressure drop distribution is discussed for both average value and uniformity. Finally, the pressure change in the main channels is quantitatively analyzed. Considering both the pressure drop of the entire bed and pressure change in the main channels, the pressure drop distribution uniformity in the particle bed is evaluated.

1. Gas-phase Flow Distribution

Under different conditions, the gas flow field has many commonalities and differences in the particle bed and main channels.

1-1. Commonalities of the Gas Flow Field under Different Conditions

In the particle bed and main channels, high solid holdup and variable mass flow appear, respectively, which shows a completely different gas phase flow field distribution: the pressure significantly changes in the particle bed, and the gas velocity significantly changes in the main channels (Fig. 4).

(a) Commonalities of the gas flow field in the particle bed

In the particle bed, the flow field distribution is uniform and regular. As indicated by Fig. 5, Fig. 6 and Fig. 7, except for the ends of the particle bed, the pressure/velocity axial distribution is uniform in the main range. In this paper, more attention is given to radial changes instead of axial changes.

The gas velocity u_{local}=Q/A is relatively low for the cylindrical flow cross-section in the particle bed and changes along the axial direction when the cross-section A=πr^2 varies. When the particles accumulate in the particle bed, the gas-solid resistance results in a large pressure drop. Along the gas flow direction, the pressure decreases, and its amplitude decreases because at the position with the small radius, the local gas velocity becomes large, and the pressure significantly changes.

(b) Commonalities of the gas flow field in the main channels

In the main channels, which are affected by various mass flows, the gas velocity changes approximately linearly in the axial direction, and the pressure also changes, as shown in Fig. 5. Based on Eq. (1), the pressure changes along the axial direction due to the momentum change caused by the increase/decrease in gas velocity, wall friction resistance, gravity, etc.

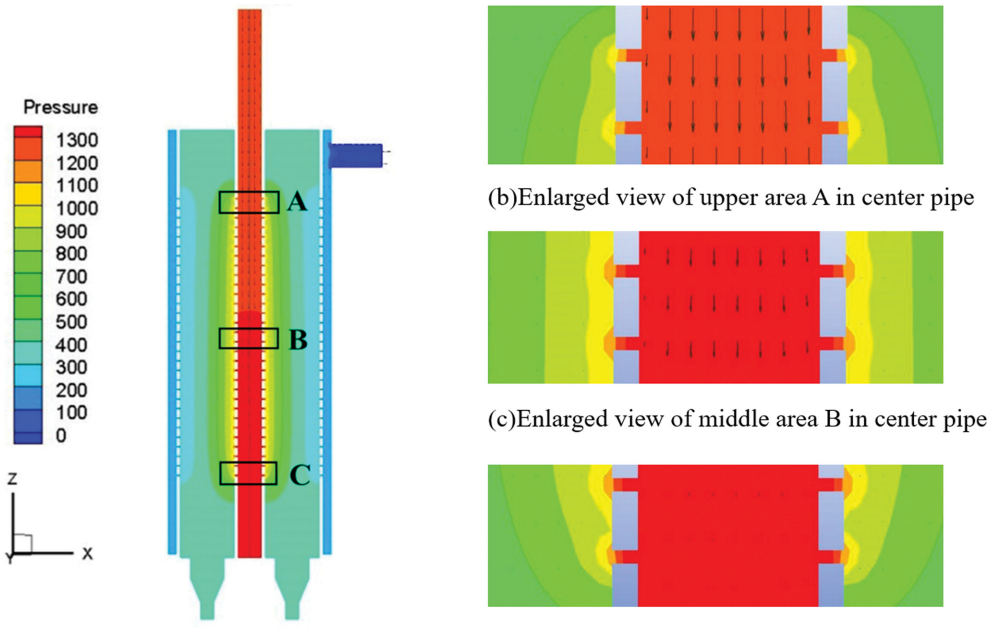

Fig. 4. Schematic diagram of pressure distribution and gas velocity vector in the CF U-type radial bed (Q=180 m^3/h, d_p=0.77exp-3 m, γ= 0.345).

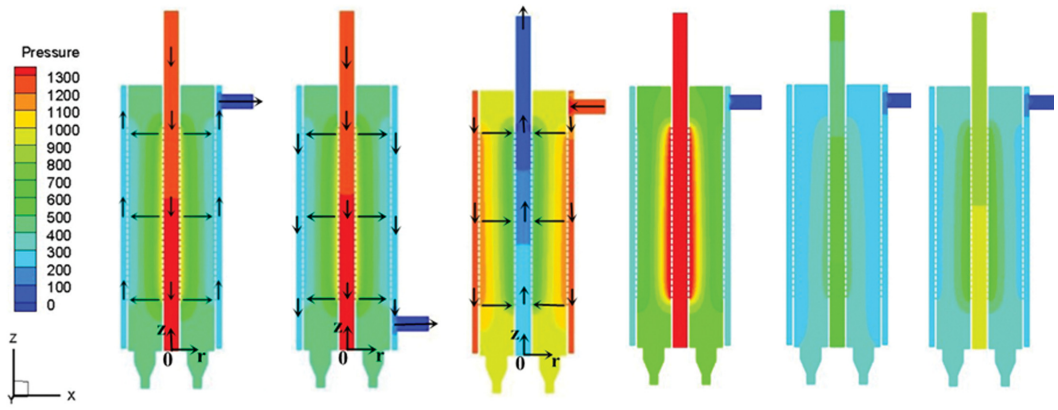

(a) Pressure distribution

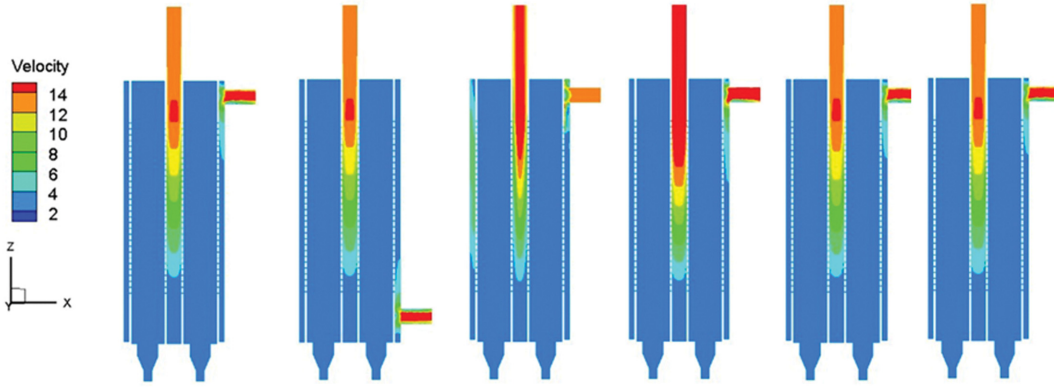

(b) Gas velocity distribution

Type	CF-U[1]	→[2] CF-Z	→ CP-U	CF-U	CF-U	CF-U
Q/(m³/h)	180	180	180	→ 240	180	180
d_p/(m)	0.77exp-3	0.77exp-3	0.77exp-3	0.77exp-3	→ 1.5exp-3	0.77exp-3
γ	0.345	0.345	0.345	0.345	0.345	→ 0.4

Fig. 5. Schematic diagram of the pressure and gas velocity distribution under different operating mode, gas flow rate, particle diameter and bed voidage.

Compared to the annular pipe, the flow field usually significantly changes in the center pipe due to its relatively small cross-sectional area A_d<<A_c and large gas velocity. In addition, at the gas inlet/outlet of the annular pipe, there are local areas with high pressure/gas velocity changes, but their effect on the entire bed is negligible. Therefore, the flow in the center pipe is mainly studied in the following section. In the centrifugal/centripetal radial bed, the center pipe is the discharge/collection channel.

In the center pipe, the gas velocity increases along the axial direction, and the pressure changes in the opposite direction in this paper. However, the variation trend and amplitude change in different radial positions. To better analyze the flow field in the center pipe, the upper, middle and lower parts of the center pipe are analyzed, as shown in Fig. 6 and Fig. 7.

The upper part of the center pipe is the initial section of a perforated flow. Along the axial direction, the gas velocity and pressure vary significantly due to their large gas velocity and near the interface between the walls with and without holes. Along the radial direction, the gas velocity distribution varies significantly: the velocity is fast in the center due to the inertial force at the gas inlet/outlet and slow near the wall, which is affected by the wall friction resistance and gas inflow/outflow. While the pressure hardly changes due to the low gas radial velocity.

The middle section is a relatively stable area of perforated flow

[1]CF-U: Centrifugal U-type flow, the gas flows centrifugally from the center pipe to the annular pipe, where the gas flow directions are different in the two channels; CF-Z: Centrifugal Z-type flow, the gas flows centrifugally from the center pipe to the annular pipe, where the gas flow directions are identical in the two channels; CP-U: Centripetal U-type flow, the gas flows centripetally from the annular pipe to the center pipe, where the gas flow directions are different in the two channels; CP-Z: Centripetal Z-type flow, the gas flows centripetally from the annular pipe to the center pipe, where the gas flow directions are identical in the two channels.

[2]→: Represent a change in a single variable, e.g., →CF-Z denotes CF-U changes to CF-Z.

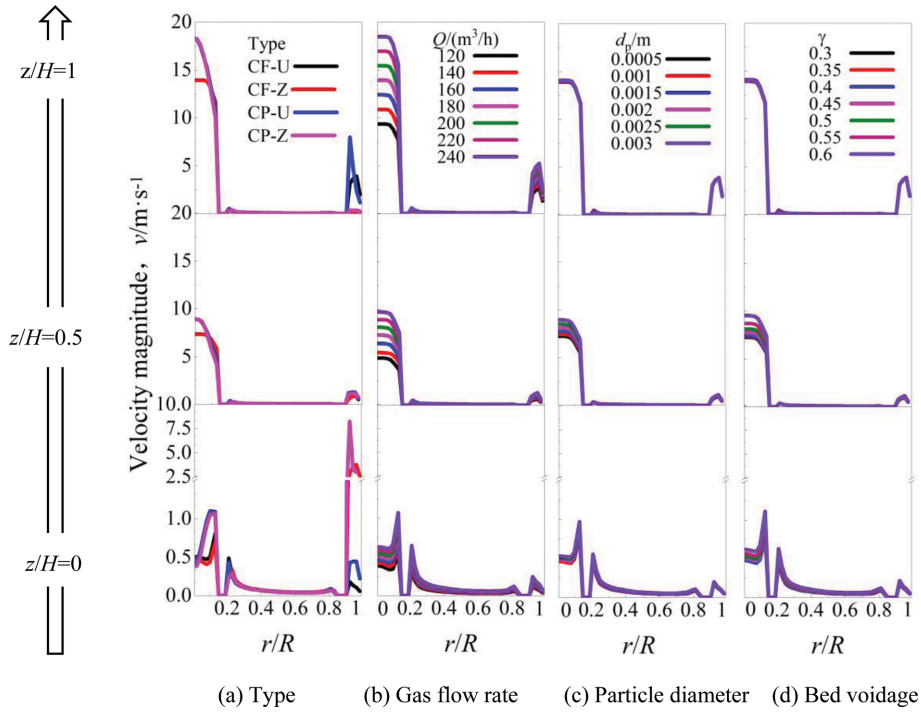

Fig. 6. Radial distribution diagram of gas velocity at each axial height z/H under different conditions.

development. The velocity and pressure are relatively stable along the axial and radial directions, which are highly representative. Compared to the upper part, the gas velocity increases more linearly and the pressure change amplitude is smaller along the axial direction, while the pressure and gas velocity change less along the radial direction.

The lower part is the end section of the perforated flow with a relatively low pressure and gas velocity. Along the axial direction, the gas velocity and pressure change slightly for the small gas velocity. In addition, a stagnation point with zero gas velocity appears near the center. Along the radial direction, the gas velocity shows a distribution with a small value in the center because there is a stagnation point and a large value in the wall due to the gas flowing into/out of the holes. While the pressure hardly changes for a small gas radial velocity.

Therefore, considering its large cross-sectional area, the flow field hardly changes in the annular pipe, and the flow field should be investigated around the center pipe and particle bed in this paper. In addition, the upper, middle and lower parts of the center pipe show different flow field distribution characteristics, which should be analyzed in detail.

1-2. Difference in the Gas Flow Field under Different Conditions

The gas flow field in the radial bed is affected by different conditions, e.g., the operating mode, gas flow rate, particle diameter and bed voidage. For example, in different operating modes, the center pipe is the discharge/collection channel, and the gas flow directions are different in the particle bed. The gas flow rate, particle diameter and bed voidage affect the gas resistance in the particle bed.

The radial bed is divided into four operating modes: centrifugal Z-type (CF-Z), centrifugal U-type (CF-U), centripetal Z-type (CP-Z), and centripetal U-type (CP-U). According to the design requirements (section 1), the gas flow rate is selected to be 120-240 m^3/h (8.66-17.33 m/s) [8] in this paper. The particle diameter is selected to be (0.5-3)exp-3 m, and the bed voidage is 0.3-0.6, which relates to the particle-to-wall size ratio, pore structure, particle shape and accumulation state.

(a) Effect of operating modes on the gas flow field

The gas velocity distribution in the particle bed hardly changes with different operating mode, since the local gas velocity $u_{local} \approx Q/(\pi r^2)$ remains almost unchanged. The pressure distribution changes with the centrifugal and centripetal operating modes. Because in the centrifugal flow, the gas flows outward through the particle bed into the atmosphere, and the pressure in the center pipe is approximately the sum of the atmospheric pressure and total pressure drop of the particle bed. In a centripetal flow, the pressure of the center pipe is approximately equal to the atmospheric pressure.

In the center pipe of the centrifugal and centripetal radial bed, both the gas velocity and pressure change along the axial direction, as shown in Fig. 5, Fig. 6 and Fig. 7. According to Eq. (1), in the discharge channel, the gas velocity gradually decreases along the flow direction. The momentum change increases the pressure, while the frictional resistance decreases it. The pressure may continue to increase, remain unchanged or decrease along the flow direction. In this paper, the pressure increases along the flow direction (axial downward), which indicates that the momentum change has a greater effect than the frictional resistance. It is a momentum exchange channel. In the collection channel, the gas velocity increases along the flow direction and both momentum and frictional resistance decrease the pressure. Therefore, under identical conditions, the pressure variation in the discharge channel is less than that in the collection channel. In the Z-type radial bed, the gas flow direc-

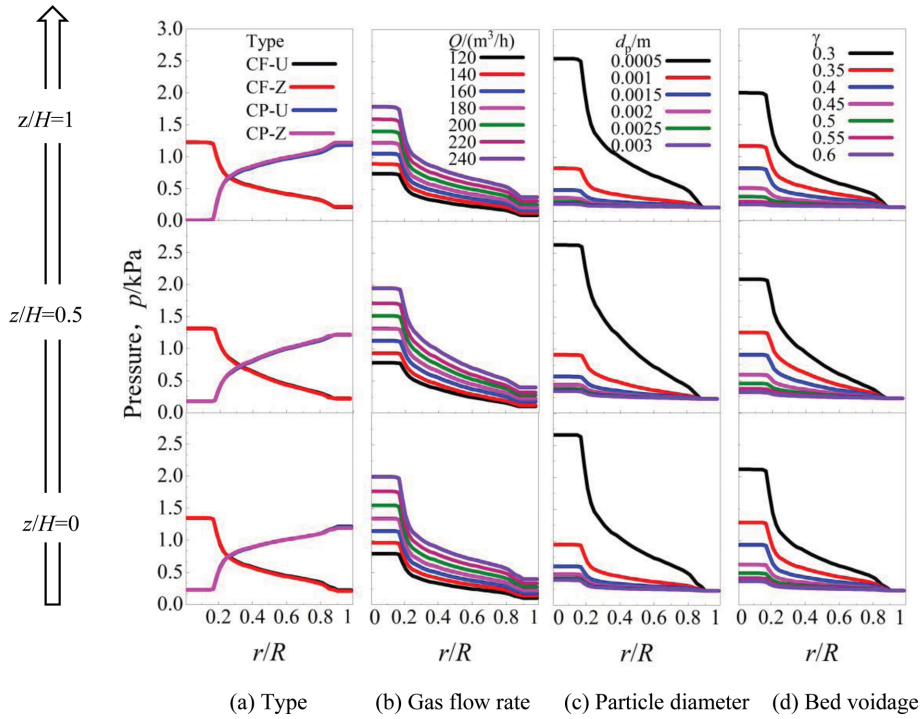

(a) Type (b) Gas flow rate (c) Particle diameter (d) Bed voidage

Fig. 7. Pressure distribution along the radial direction at each axial height z/H under different conditions.

tion is identical in the center and annular pipes. Therefore, in the momentum exchange channel, along the gas flow direction, the pressure in the discharge channel always increases, and the pressure in the collection channel decreases. For the Z-type structure, the identical flow direction makes the pressure difference between two channels increase faster than the U-type structure whose opposite flow direction makes the pressure difference between two channels offset part of each other.

In the upper, middle, and lower parts of the center pipe, the gas velocity and pressure change with the centrifugal and centripetal operating modes. Due to the gas inflow/outflow form in the center pipe, compared to the centrifugal flow, the gas velocity changes more along the radial direction, and the pressure changes less in the centripetal flow. In the upper, middle, and lower parts of the center pipe, the gas velocity and pressure have a small correlation with the U- and Z-types because of the small change in pressure of the annular pipe (section 3.1.1).

In the CF-U radial bed, both pressure drop axial and gas velocity radial distribution become more uniform in the particle bed. Thus, the analysis was conducted under different gas flow rate, particle diameter and bed voidage.

(b) Effect of the gas flow rate on the gas flow field

With increasing the gas flow rate, both gas velocity and pressure increase in the particle bed and center pipe of the CF-U radial bed. This is because the local gas velocity increases in all parts of the bed as well as the gas-solid resistance in the particle bed, as shown in Fig. 6 and Fig. 7.

In the upper, middle and lower parts of the center pipe, the gas velocity and pressure increase with an increasing gas flow rate, and their distributions change slightly. The axial variation amplitudes of the gas velocity and pressure also increase, due to the increase in amount of gas outflow from the holes.

(c) Effect of the particle diameter and bed voidage on the gas flow field

With the decrease in particle diameter and bed voidage, the gas superficial velocity hardly changes, since it is approximately proportional to the total gas flow rate. The pressure increases at each position, as shown in Fig. 6 and Fig. 7. Because the actual gas velocity $u_r=u_g/\gamma$ and gas-solid contact area $S_{g\text{-}s}=V(1-\gamma)/(1/6\pi d_p^3)\times\pi d_p^2=6V(1-\gamma)/d_p$ in the particle bed increase at the moment, which increases the gas-solid resistance, radial variation amplitude and total pressure drop.

In addition, the increase of total pressure drop in the particle bed makes the gas velocity axial distribution in the bed more uniform, which affects the gas velocity axial distribution in the center pipe. In the upper part of the center pipe, the gas velocity distribution along the radial direction is mainly affected by the inertial force of the inlet gas velocity, and the gas velocity distribution hardly changes with the particle diameter and bed voidage. At the middle part and lower part, affected by the gas velocity axial distribution in the bed, the gas axial velocity slightly decreases.

2. Pressure Drop Distribution and Nonuniformity in the Particle Bed

The pressure drop distribution in the particle bed is affected by different conditions. The pressure drop distribution is qualitatively analyzed by the nonuniformity index. The internal influencing factors are also discussed.

2-1. Pressure Drop Distribution in the Particle Bed

The total pressure drop of the particle bed includes the pressure drop of the gas perforation in the Johnson net and particle bed, as shown in Fig. 8(a). The gas perforation pressure drop mainly depends on its structure and gas phase parameters. The gas perfo-

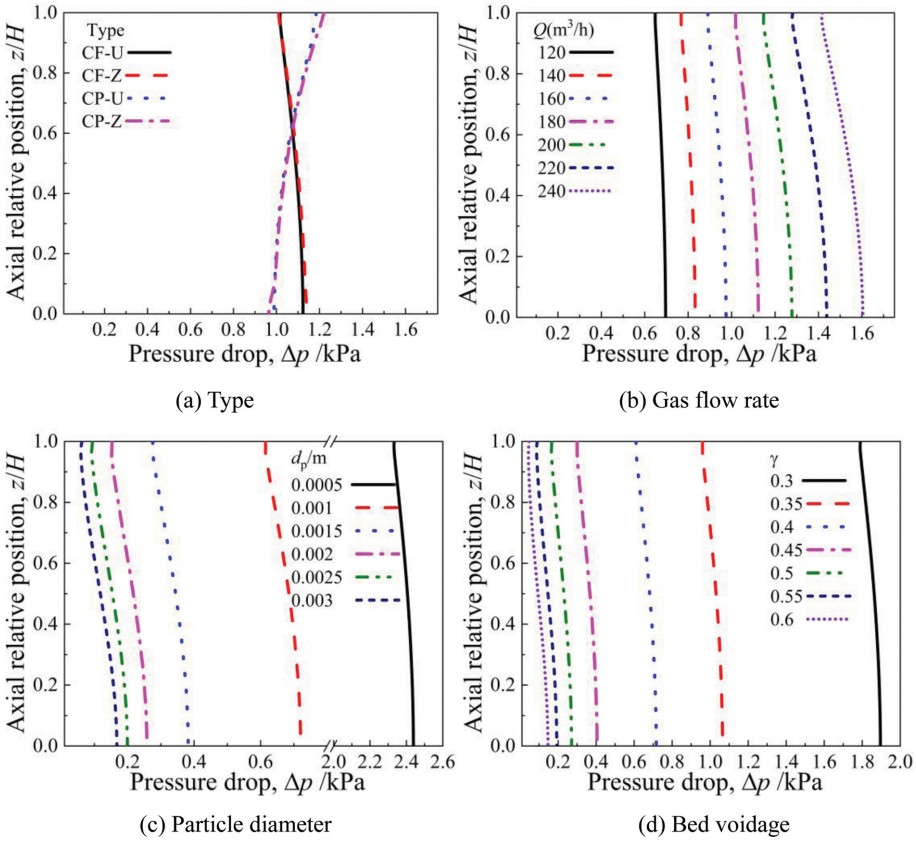

(a) Type (b) Gas flow rate

(c) Particle diameter (d) Bed voidage

Fig. 8. Changes in pressure drop of a radial bed particle bed with different operating mode, gas flow rate, particle diameter, and bed voidage.

ration pressure drop remains unchanged under different operating mode, particle diameter and bed voidage because the local gas velocity flow through holes hardly changes, while the gas perforation pressure drop increases when the gas flow rate increases. Due to the large porosity and smaller thickness of the Johnson net, the perforation pressure drop is always less than 0.7% of the pressure drop in the particle bed, which is negligible here. Therefore, the total pressure drop of the particle bed is approximately equal to the pressure drop of the particle bed.

(a) Pressure drop axial distribution in the particle bed

The pressure drop axial distribution is greatly affected by the centrifugal and centripetal flows. Because in a momentum exchange channel (section 3.1.2), the pressure decreases along the axial direction in the center pipe in the centrifugal bed, while the pressure decrease is opposite in the centripetal bed. The pressure drop axial distribution is less affected by the U- and Z-types due to the small effect of the annular channel, as shown in Fig. 8(a).

With an increasing gas flow rate, particle diameter and bed

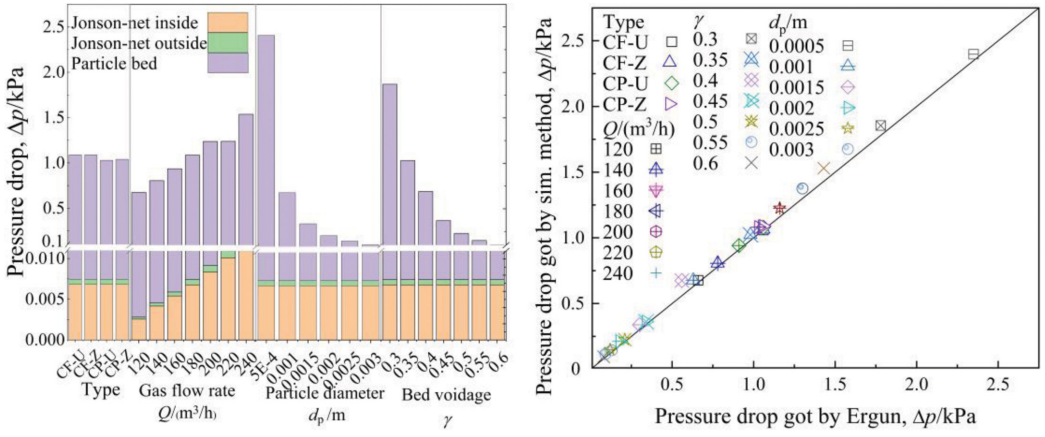

(a) Proportion of each part (b) Comparison of simulated and theoretical results

Fig. 9. Proportion diagram of each part in particle bed and its theoretical calculation.

voidage, the pressure drop of the particle bed increases, but its axial distribution trend does not significantly change, as shown in Fig. 8(b)-(d), since the change in actual gas velocity or gas-solid contact area in the particle bed (Section 3.1.2) increases the gas-solid resistance.

(b) Average pressure drop of the particle bed

Similar to the pressure drop distribution, the average pressure drop of the particle bed is less affected by the operating mode and increases with an increasing gas flow rate or decreasing particle diameter and bed voidage. We assume that the flow in the particle bed is a uniform plug flow. According to the Ergun formula, the calculus operation is performed and Eq. (12) is obtained. According to Fig. 9(b), this calculus formula has a good correlation with the simulation results, except for the small deviation caused by the gas axial dispersion in the particle bed. Thus, in studies of the pressure drop in the particle bed, uniform plug flow can be assumed. The accuracy of the simulation results is verified again to have a good correlation with the traditional Ergun formula [34]. Moreover, this calculus formula can be used to predict the pressure drop of the particle bed in a radial bed.

$$\Delta p = \int_{r_1}^{r_2}\left[\frac{150(1-\gamma)^2\mu}{d_p\gamma^3}\cdot\frac{Q}{2\pi rH}+1.75\frac{1-\gamma}{d_p\gamma^3}\rho g\left(\frac{Q}{2\pi rH}\right)^2\right]dr = \frac{150(1-\gamma)^2\mu}{d_p 2\gamma^3}\cdot\frac{Q}{\pi H}\ln\frac{r_2}{r_1}+1.75\frac{1-\gamma}{d_p\gamma^3}\rho g\left(\frac{Q}{\pi H}\right)^2\left(\frac{1}{r_1}-\frac{1}{r_2}\right) \quad (12)$$

2-2. Nonuniform Index of the Pressure Drop Distribution in the Particle Bed

With the nonuniform index of the pressure drop distribution η Eq. (13), the uniformity of the pressure drop axial distribution in the particle bed is analyzed. In the formula, the numerator is the variance of the pressure drop axial distribution, and the denominator is the average pressure drop of the particle bed. Hence, η is affected by the pressure change of the main channels and average pressure drop of the particle bed, which decreases with the decrease in the former channel and the increase in the latter channel. A smaller η corresponds to a more uniform pressure drop axial distribution.

$$\eta = \frac{\sqrt{\sum_{i=1}^{m}(\Delta p_i-\Delta\bar{p})^2/(m-1)}}{\Delta\bar{p}},\ \Delta\bar{p}=\sum_{i=1}^{m}\Delta p_i/m \quad (13)$$

As shown in Fig. 10, the CF-U radial bed has the smallest η and the most uniform pressure drop distribution. Because when the gas flow rate remains unchanged, the average pressure drop of the particle bed does not greatly change. η is mainly related to the pressure change in the main channels. According to Eq. (1), the CF-U radial bed has the smallest pressure change of the main channel in the momentum exchange channel (section 3.1.2).

With an increasing gas flow rate, η increases slightly and the uniformity of the pressure drop axial distribution worsens. According to Eq. (12) and Eq. (1), with an increasing gas flow rate, both the average pressure drop of the particle bed and axial change amplitude of pressure in the center pipe increase, which are approximately 1-2 or 2 powers of the gas flow rate. Both the average pressure drop of the particle bed and pressure change in the main channel increase, but the former significantly increases, which slightly increases η.

With a decreasing particle diameter and bed voidage, η decreases and the uniformity of the pressure drop axial distribution improves, because according to Eq. (12) and Eq. (1), the pressure drop of the particle bed is the −1 power of the particle diameter and −1~−3 power of the bed voidage. Although it is affected by the pressure drop of the particle bed, the change in pressure in the center pipe is relatively small because the gas flow rate remains almost unchanged, which makes η decrease.

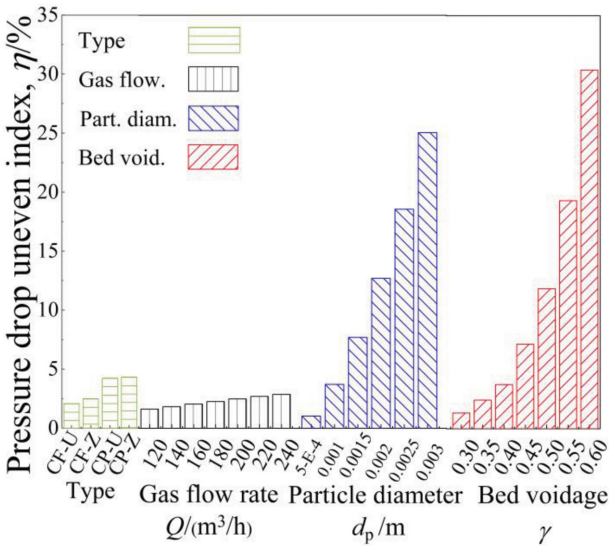

Fig. 10. Nonuniform index of pressure drop distribution in the bed under different conditions.

3. Global and Local Momentum Exchange Coefficients

The pressure drop axial distribution of the particle bed depends on the combined effect of the pressure drop in the particle bed and axial change in pressure in the center pipe. The former can be calculated by Eq. (12). The pressure change of the center pipe along the axial direction can be approximately calculated by Eq. (1), which contains the momentum exchange coefficient. The momentum exchange coefficient should be further investigated under different conditions and its internal generated causes must be studied.

3-1. Calculation Method for the Momentum Exchange Coefficients

When calculating the momentum exchange coefficient k, it is necessary to select two axial heights (z=i, i+1). Within these two axial heights, Eq. (1) is integrated into Eq. (14), and k can be derived from the pressure, gas velocity and variation amplitude. To ensure the accuracy of the calculation, the cross-section average method is adopted in the simulation.

$$k = \frac{-\Delta p/\Delta z \mp \rho g\left(\frac{u_{i+1}+\Delta u/2}{u_i}\right) \pm \frac{\lambda}{2D_e}\rho\frac{(u_i+u_{i+1})^2}{4}(1-\phi)}{\rho\Delta u^2/\Delta z} \quad (14)$$

When calculating the global k, the two axial positions are selected as the top and bottom height positions of the Johnson net, i.e., z=0, H, where $u_i=u_0$, $u_{i+1}=0$, $\Delta z=H$. When calculating the local k, 31 axial heights are selected uniformly along the height range of the Johnson net, and the height is far away from the hole area to

avoid its effect on the calculation. The local k at each adjacent axial height is calculated and its axial distribution is presented.

3-2. Internal Generation Factors of the Momentum Exchange Coefficients

With the idealized derivation, the momentum exchange coefficient k should be 0.5 and 1 in the discharge/collection channels. However, the actual situation is different, considering the effect of gas perforation on wall resistance and the presence of the gas axial velocity after perforation.

(a) Effect of the wall conditions on the momentum exchange coefficients

In Eq. (14), the wall friction resistance is $\lambda/(2D_e)\cdot\rho\cdot(u_i+u_{i+1})^2/4\cdot(1-\phi)$ under the nonslip boundary condition (u_w=0), and it changes along the axial direction when the gas velocity changes. When the wall shear resistance τ is 0 (free boundary condition), 0.1 and 1 N/m^2, the wall friction resistance is always constant: $(1-\phi)\cdot 2\pi r_1\tau/\pi r_1^2=2(1-\phi)\tau/r_1$, and it does not change with the axial position. Accordingly, the global and local momentum exchange coefficients k can be obtained.

As shown in Fig. 11(a), under the nonslip boundary condition, the local k axial distribution is more uniform. For the remainder, with the increase in wall resistance, the global k and local k increase. The local k axial distribution worsens with greater changes in the lower part of the center pipe because the boundary layer of the pipe wall is relatively stable when the wall shear resistance is fixed, as shown in Fig. 11(b).

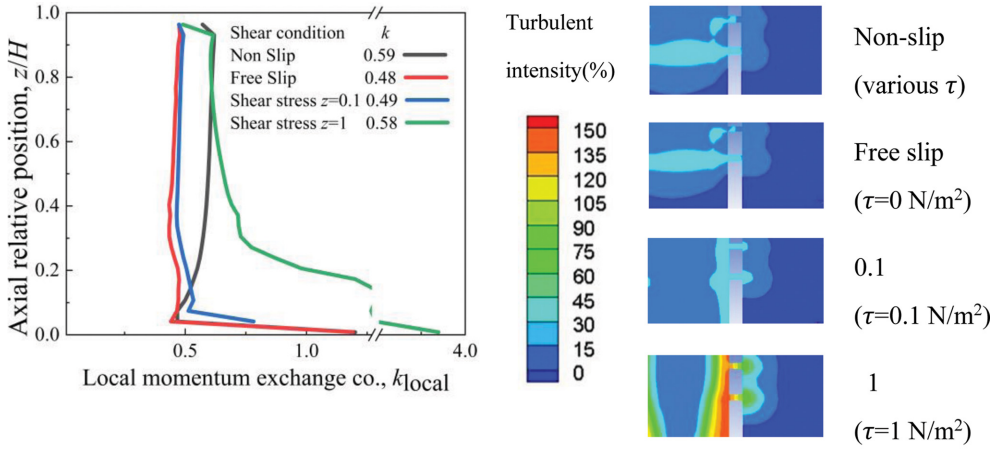

(a) Global and local momentum exchange coefficients distribution

(b) Turbulence intensity distribution at z/H=0 on the right side of area C in Fig. 4

Fig. 11. Momentum exchange coefficient and local turbulence intensity distribution at the bottom of the center pipe under different wall conditions in the CF-U type radial bed (Q=180 m^3/h, d_p=0.77exp-3 m, γ=0.345).

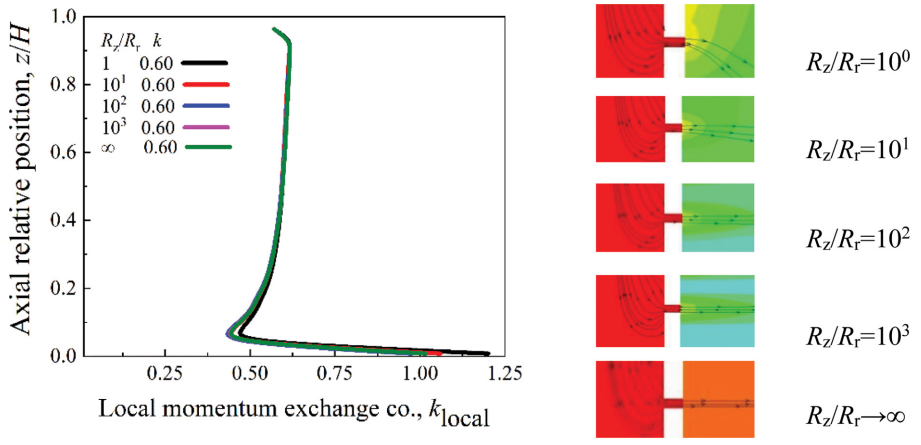

(a) Global and local momentum exchange coefficients distribution

(b) Gas streamline diagram at z/H=0 on the right side of area C in Fig. 4

Fig. 12. Momentum exchange coefficient and gas streamlines at the bottom of the center pipe under different radios of the axial/radial resistance coefficient in the CF-U type radial bed (Q=180 m^3/h, d_p=0.77exp-3 m, γ=0.345).

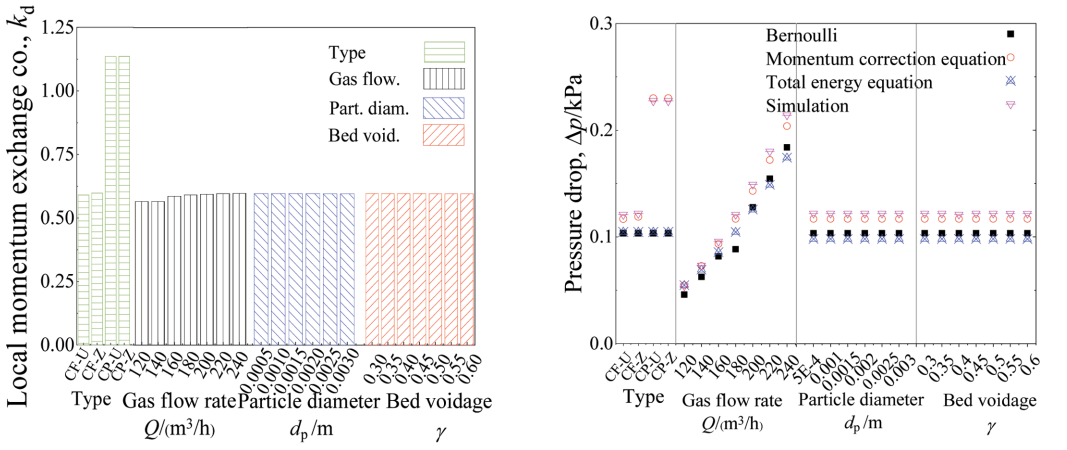

(a) Global momentum exchange coefficient

(b) Axial pressure drop under different calculation methods

Fig. 13. Global momentum exchange coefficient and axial pressure drop under different conditions in the discharge channel.

(b) Effect of the gas-solid axial resistance on the momentum exchange coefficients

The ratio of the gas-solid axial to radial resistance in the particle bed is changed to 10^0 (the original condition), 10^1, 10^2, 10^3 and ∞. With the increase in the ratio, the flow of the gas in the axial direction becomes increasingly difficult and the gas axial velocity decreases. At infinity, the gas flows only along the radial direction and the axial gas velocity is approximately zero, as shown in Fig. 12(b).

As shown in Fig. 12(a), under different ratios, the global and local momentum exchange coefficients k do not greatly change and only slightly vary in the lower part of the center pipe. The particle bed of the radial bed has axial diffusion [35], so the gas axial velocity is mainly at the ends of the bed, which may affect k in the upper and lower parts of the center pipe. In the upper part of the center pipe, the gas velocity is relatively large and the gas axial velocity after perforation hardly affects k. At the lower part of the center pipe, the gas velocity is small and k decreases with an increasing ratio, which indicates that the effect of the gas axial velocity on the flow field after perforation mainly affects k in the lower area of the center pipe.

3-3. Global Momentum Exchange Coefficient

As shown in Fig. 13(a), the global momentum exchange coefficient k is more affected by the centrifugal and centripetal operating modes and less affected by the U- and Z-types. In the centrifugal/centripetal bed, the center pipe is the discharge/collection channel, and k is less/greater than 1, which is similar to the results of Zhang et al. [8].

With the increase of the gas flow rate or the decrease of the particle diameter and bed voidage, the global k increases slightly. Because the change in the total gas flow rate and pressure drop of the particle bed inevitably change the flow field of the center pipe, which is reflected in k. But its effect is limited. The coefficient is most affected by the centrifugal and centripetal operating modes, then followed by the gas flow rate and particle diameter/bed voidage.

Fig. 13(b) indicates that in contrast to the Bernoulli and total energy equations, the pressure variation obtained by the momentum correction equation has good correlation with the simulation data.

3-4. Local Momentum Exchange Coefficient

At each axial position, the change trend of the local momentum exchange coefficient k is identical to the change trend of the global k under different operating mode, gas flow rate, particle diameter and bed voidage, as shown in Fig. 14.

Under different conditions, the local k axial distribution does not change significantly and shows a decreasing-increasing-decreasing trend along the axis. However, at the local axial position of the center pipe, the local k axial distribution changes with different conditions. In the upper part of the center pipe of the CF-U bed, the flow field is greatly affected by the inlet inertial force with high gas velocity and located at the junction area between the walls with

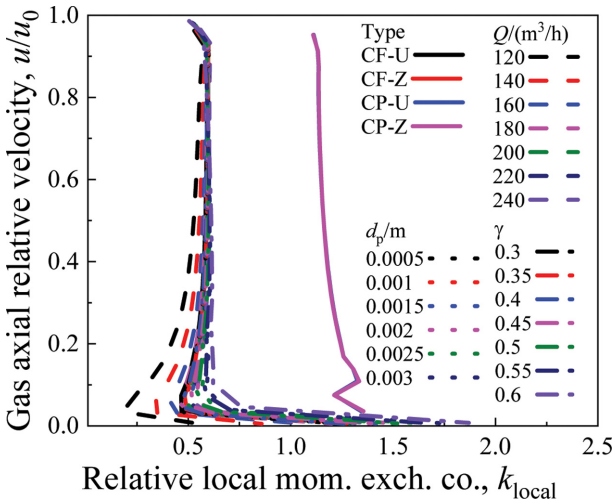

Fig. 14. Distribution diagram of the local momentum exchange coefficient with the velocity ratio under different conditions in the center pipe of the radial bed.

and without holes, so the local k hardly changes with the conditions. In the middle of the center pipe, the flow is relatively stable and the local k varies less with different conditions. In the lower part of the center pipe, the flow field is greatly affected by the low gas velocity and the presence of a gas stagnant zone. The local k easily increases with an increasing gas flow rate or decreasing particle diameter and bed voidage.

CONCLUSIONS

The gas flow field in the radial bed was simulated by both Euler single-phase flow and porous media models. A grid size of 0.01 m and the k-ε RNG model were selected. After model verification, the flow field was systematically investigated under different conditions (operating mode, gas flow rate, particle diameter, bed voidage, wall shear condition, and ratios of the gas-solid axial/radial resistance). The pressure drop axial distribution was discussed and the main conclusions are as follows.

(1) In the particle bed and main channels, high solid holdup and gas variable mass flow occur, respectively, which cause different changes in the flow field. The gas velocity in the bed is low, but the particles have greater resistance to the gas and produce a large pressure drop. The gas velocity in the main channel is high, and the pressure will significantly change due to factors such as momentum exchange, friction resistance and gravity. In addition, different flow states appear in the upper, middle and lower parts of the main channel. The upper part of the high-gas-velocity section is greatly affected by the gas inertia force and junction area between the walls with and without holes, the middle part is relatively stable and the lower part is affected by the gas stagnation zone.

(2) According to the nonuniform index of the pressure drop axial distribution, the pressure drop axial distribution is improved with increasing the particle bed pressure drop or decreasing the pressure change in the main channels. The CF-U radial bed has a more uniform pressure drop distribution: the momentum exchange/friction resistance terms in the momentum exchange channel and the pressure in the center/annular pipes cancel each other out. With increasing the gas flow rate or decreasing the particle diameter and bed voidage, the bed pressure drop becomes larger than the pressure change in the main channels, and the pressure drop distribution becomes more uniform.

(3) The total pressure drop of the particle bed includes the pressure drop of the particle bed and gas perforation of the Johnson net. Comparing the flow field in the bed with/without particles, the gas perforation pressure drop is found to mainly relate to the gas flow rate and structure. Due to the higher porosity of the Johnson net, the gas perforation pressure drop can be ignored here. Thus, the total pressure drop of the particle bed is approximately equal to the pressure drop of the particle bed, which can be well calculated by the Ergun equation.

(4) For the main channels, only the pressure change in the center pipe should be considered when the center pipe has a smaller cross-sectional area than that in the annular pipe. The pressure change in the center pipe can be calculated by the equation with the momentum exchange coefficient k. By changing the wall shear conditions and the ratio of gas axial/radial resistance, the internal generation factors of k are found to result from the influence of gas perforation on the boundary layer and the existence of the gas axial velocity after perforation. In addition, the global and local k slightly increase with increasing gas flow rate or decreasing particle diameter and bed voidage, while the local k relates to the velocity ratio or axial position. Under different conditions, k does not greatly change at the high gas velocity end for the existence of a high gas inertia force and the junction area, but changes significantly at the low gas velocity end due to the existence of the gas stagnation zone.

ACKNOWLEDGEMENTS

The authors gratefully acknowledge the financial support by the State Key Laboratory of Heavy Oil Processing (grant number SKLOP201903002), the Natural Science Foundation of Hebei (grant number B2017202185) and the College Student Innovation and Entrepreneurship Training Program Project of Hebei University of Technology (grant number X202010080006).

NOMENCLATURE

A : gas flow cross sectional area [m^2]
A_d : sectional area of discharge channel [m^2]
A_c : sectional area of collection channel [m^2]
C_2 : the inertial resistance factor [m^{-1}]
$C_{1\varepsilon}$, $C_{2\varepsilon}$, $C_{3\varepsilon}$: constant, respectively 1.44, 1.92, 0.09
D_e : inner diameter of center pipe [m]
d_p : particle diameter [m]
d′ : absolute roughness of pipe wall [m]
g : gravity acceleration [m/s^2]
G_k : the generation of turbulence kinetic energy due to the mean velocity gradients [$kg/(m \cdot s^3)$]
G_b : the generation of turbulence kinetic energy due to buoyancy [$kg/(m \cdot s^3)$]
H : center pipe height [m]
k : momentum exchange coefficient
k_{local} : local momentum exchange coefficient
k_d : the global momentum exchange coefficient in the center pipe
p : pressure [pa]
Q : volumetric gas flow rate [m^3/h]
Re : Reynolds number
R_r : radial resistance coefficient in the particle bed
R_z : axial resistance coefficient in the particle bed
R_ε : the additional term [$kg/(m \cdot s^3)$]
r : diameter of particle bed [m]
r_1 : inner diameter of particle bed [m]
r_2 : outer diameter of particle bed [m]
$S_{g\text{-}s}$: gas-solid contact area [m^2]
S_i : porous media source term [$kg/(m \cdot s^3)$]
t : time [s]
u : fluid superficial velocity in the main channel [m/s]
u’ : gas superficial velocity in main channel before gas perforation [m/s]
u” : gas superficial velocity in main channel after gas perforation [m/s]

u' : fluctuating velocity [m/s]
u_0 : gas inlet velocity [m/s]
u_{local} : local gas velocity [m/s]
u_g : gas superficial velocity [m/s]
u_w : gas superficial velocity on the wall [m/s]
u_r : actual velocity [m/s]
V : volume [m^3]
Y_m : the contribution of the fluctuating dilatation in compressible turbulence to the overall dissipation rate [kg/(m·s^3)]

Greek Symbols

ρ : fluid density [kg/m^3]
ρ_g : gas phase density [kg/m^3]
λ : friction resistance coefficient
ϕ : Johnson net porosity
μ : viscosity [kg/(m·s)]
μ_t : turbulence viscosity coefficient
μ_{eff} : effective viscosity [kg/(m·s)]
γ : bed voidage
τ : wall shear resistance [N/m^2]
$\bar{\bar{\tau}}$: stress tensor [pa]
$\bar{\bar{I}}$: identity matrix [pa]
ε : the turbulence dissipation rate [m^2/s^3]
κ : the turbulence kinetic energy [m^2/s^2]
α : porous media permeability
$1/\alpha$: viscous resistance coefficient
α_k : the turbulent Prandtl numbers for κ
α_ε : the turbulent Prandtl numbers for ε
η : nonuniform index of the pressure drop distribution

REFERENCES

1. R. J. Li and Z. B. Zhu, *Chem. React. Eng. Technol.*, **24**, 368 (2008).
2. D. Y. Fang and Z. B. Zhu, *Chem. Eng.*, **29**, 18 (2001).
3. W. M. Liu and X. D. Liu, *Pet. Chem. Equip. Technol.*, **27**, 56 (2006).
4. S. Md, H. Md, C. M. A. A. and M. Md, *J. King Saud Univ. - Eng. Sci.*, **29**, 21 (2020).
5. X. J. Dong, Y. J. He, J. N. Shen and Z. F. Ma, *Chem. Eng. Sci.*, **175**, 306 (2018).
6. W. L. Liu and X. Li, *Chem. Eng. Sci.*, **191**, 525 (2018).
7. S. Y. Chin, A. Hisyam and H. Prasetiawan, *Int. J. Chem. React. Eng.*, **14**, 33 (2016).
8. C. F. Zhang, Z. B. Zhu, M. S. Xu and B. C. Zhu, *J. Chem. Ind. Eng.*, 67 (1979).
9. O. Nekhamkina and M. Sheintuch, *Chem. Eng. J.*, **372**, 277 (2019).
10. N. Minocha and J. B. Joshi, *Int. J. Heat Mass Transf.*, **151**, 119420 (2020).
11. N. Gilmore, A. Hassanzadeh-Barforoushi, V. Timchenko and C. Menictas, *Appl. Therm. Eng.*, **183**, 116227 (2021).
12. R. J. Li, C. Y. Chen, Y. Q. Wu and Z. B. Zhu, *Chem. Eng.*, **10**, 28 (2009).
13. X. Zhang, J. Lu, L. Qiu, X. Zhang and X. Wang, *Chinese J. Chem. Eng.*, **21**, 494 (2013).
14. Y. Li, H. Si, B. Wang, X. Lu and X. J. Wu, *Korean. J. Chem. Eng.*, **35**, 835 (2018).
15. Y. Jin, Z. Q. Yu and Z. F. Sun, *J. Chem. Ind. Eng.*, 203 (1984).
16. X. Q. Song, Z. W. Wang and Y. Jin, *J. Chem. Ind. Eng.*, **43**, 268 (1992).
17. H. Wei, R. Wang, D. Wang, T. Wu, Y. Liu and S. Zhang, *Chinese J. Process Eng.*, **20**, 1406 (2020).
18. Z. G. Xu, F. Yu, R. J. Li, Z. B. Zhu, R.J . Li and C. F. Zhang, *Chinese J. Process Eng.*, **3**, 1 (2003).
19. X. L. Zhang, F. X. Zhao, J. Fan and B. Z. Li, *J. Northwest Univ.: Nat. Sci. Ed.*, **26**, 235 (1996).
20. H. Wang and X. Y. Gu, *Chem. Eng.*, **46**, 36 (2018).
21. Z. Mu, J. Wang, T. Wang and Y. Jin, *Chem. Eng. Process*, **42**, 409 (2003).
22. J. F. Wang, S. Jing, T. F. Wang, Y. Jin, X. Q. Ma and L. P. Gao, *J. Chem. Eng. Chin. Univ.*, **13**, 435 (1999).
23. M. M. S. Al-Azawii, D. Jacobsen, P. Bueno and R. Anderson, *Appl. Therm. Eng.*, **180**, 115804 (2020).
24. R. Y. Hong and H. Z. Li, *Chinese J. Process Eng.*, **17**, 367 (1996).
25. Z. R. Zhu, X. D. Liu, L. X. Jiang, Y. T. Gu, T. Peng, J. J. Yin, M. H. Liu and W. Jiang, *Chinese J. Process Eng.*, 10.12034/j.issn.1009-606X.220288.
26. L. Amiri, S. A. Ghoreishi-Madiseh, F. P. Hassani and A. P. Sasmito, *Powder Technol.*, **356**, 210 (2019).
27. A. A. Kareeri, H. D. Zughbi and H. H. Al-Ali, *Ind. Eng. Chem. Res.*, **45**, 2862 (2006).
28. Y. Y. He and Y. X. Zhang, *Chem. React. Eng. Technol.*, **35**, 200 (2019).
29. U. K. Zhapbasbayev, G. I. Ramazanova and O. B. Kenzhaliev, *Thermophys Aeromech+*, **22**, 229 (2015).
30. F. Mousazadeh, H. E. A. V. D. Akker and R. F. Mudde, *Chem. Eng. J.*, **207-208**, 675 (2012).
31. F. Z. Xiao, H. Chen and Z. H. Luo, *Can. J. Chem. Eng.*, **93**, 1033 (2015).
32. Z. Dai, M. Yu, D. Rui, X. Zhang and Y. Zhao, *Chinese J. Chem. Eng.*, **26**, 484 (2018).
33. Y. Li, M. Wang, X. Cao and Z. Geng, *Korean J. Chem. Eng.*, **37**, 839 (2020).
34. M. Zhang, H. Dong and Z. Geng, *Powder Technol.*, **354**, 19 (2019).
35. R. Wang, Y. Fan and C. Lu, *Ind. Eng. Chem. Res.*, **56**, 12203 (2017).